International Journal of Disaster Risk Science (2023) 14:600–617
https://doi.org/10.1007/s13753-023-00502-0

www.ijdrs.com
www.springer.com/13753

ARTICLE

Effects of Tectonic Setting and Hydraulic Properties on Silent Large-Scale Landslides: A Case Study of the Zhaobishan Landslide, China

Shufeng Tian[1,2,3] · Guisheng Hu[1,3] · Ningsheng Chen[1,3,4] · Mahfuzur Rahman[5,6] · Huayong Ni[7] · Marcelo Somos-Valenzuela[8]

Accepted: 20 July 2023 / Published online: 24 August 2023

Abstract

Unlike strong earthquake-triggered or heavy rainfall-triggered landslides, silent large-scale landslides (SLL) occur without significant triggering factors and cause unexpected significant disaster risks and mass casualties. Understanding the initiation mechanism of SLLs is crucial for risk reduction. In this study, the mechanism of the Zhaobishan SLL was investigated, and the SLL was jointly controlled by weak-soil (fractured rock mass) and strong-water (abundant water replenishment) conditions under the impact of active tectonism and complex hydraulic properties. Strong tectonic uplift, high fault density, and historical earthquakes led to weak-soil conditions conducive to the Zhaobishan SLL. The combined effect of unique lithology, antiform, and cultivated land contributed to the water replenishment characteristics of extensive runoff confluence (3.16 times that of the landslide body) and supported long-distance groundwater replenishment, thereby forming strong-water conditions for the landslide. The amplified seepage amount caused the strength of the soil mass on the sliding surface to decrease to 0.4 times its initial strength, eventually triggering the Zhaobishan SLL, which occurred 4.6 days after the peak rainfall. Moreover, the landslide deposits have accumulated on the semi-diagenetic clay rock, thereby controlling the subsequent recurring debris flows in the Lengzi Gully. To reduce disaster risk of SLL in vulnerable mountainous regions, the water confluence area behind the main scarp of the landslides and the hysteresis characteristics between landslides and peak rainfall should be further considered, and recurring debris flows following massive landslides also should be focused.

Keywords Debris flow · Hydraulic properties · Risk reduction · Runoff amplification · Silent large-scale landslides (SLL) · Tectonic setting

✉ Guisheng Hu
huguisheng@imde.ac.cn

✉ Ningsheng Chen
chennsh@imde.ac.cn

[1] Key Lab of Mountain Hazards and Surface Processes, Institute of Mountain Hazards and Environment, Chinese Academy of Sciences, Chengdu 610299, China

[2] University of Chinese Academy of Sciences, Beijing 100049, China

[3] Academy of Plateau Science and Sustainability, Xining 810016, China

[4] Kathmandu Center for Research and Education, Chinese Academy of Sciences-Tribhuvan University, Beijing 100101, China

[5] Department of Civil Engineering, International University of Business Agriculture and Technology (IUBAT), Dhaka 1230, Bangladesh

[6] Department of Civil Engineering, Kunsan National University, Gunsan 54150, Republic of Korea

[7] Institute of Exploration Technology, China Geological Survey, Chengdu 611734, China

[8] Department of Forest Sciences, Faculty of Agriculture and Environmental Sciences, Universidad de La Frontera, 4780000 Temuco, Chile

1 Introduction

Every year, large-scale landslides and debris flows cause thousands of deaths and economic losses of billions of dollars because of global climate change, rapid infrastructure development, and population growth within mountainous regions (Huang and Fan 2013; Handwerger et al. 2016; Pascal et al. 2020). Numerous researchers have studied the formation mechanism, triggering factors, and development conditions of such landslides. Some studies have revealed that strong earthquakes can directly trigger coseismic landslides (Gorum et al. 2011; Parker et al. 2011; Zhang et al. 2019) and debris flows (Zhang et al. 2014; Fan et al. 2018; Tian et al. 2020b). For example, Zhang et al. (2014) opined that the debris flow caused by coseismic landslides following an earthquake has the following criteria: the height difference between the landslide in the source area and the mouth of the debris flow gully is greater than 350 m, accumulation volume of landslide deposits is more than 1.0×10^6 m^3, and slope of the debris flow channel is higher than 27%. Landslides can also be associated with strong earthquakes and heavy rainfall (Malamud et al. 2004; Ram et al. 2019). Rockslides are closely associated with the tectonic environment. For example, studies in the Alps (Carlini et al. 2016; 2017), the Tien Shan Mountains (Strom and Korup 2006), and the Zagros Mountains in northern West Asia (Bahrami et al. 2019) have all revealed that geological factors, such as faults, lithology, back-shaped structures, and extensional structures, control the formation of landslides. However, a unique type of landslide with no evident triggering factors such as strong earthquakes or heavy rainfall, and the occurrence time lags behind the peak rainfall, was called silent large-scale landslide (SLL) here. Our insufficient understanding and underestimation of the potential of SLLs could lead to mass casualties in mountainous areas globally.

Landslides have been classified according to the differences in landslide velocity, volume, landslide-forming material types, and so on (Evans 2011; Hungr et al. 2014). The SLL mentioned here refers to a special class of slow-moving landslides with a volume greater than 1 million m^3 and without major triggering factors such as strong earthquakes or heavy rainfall at the time of landslide occurrence. Based on the presence or absence of obvious triggers at the time of landslide occurrence, the authors argue that landslides can be classified as those that were generated after a major triggering event, for example, an earthquake or heavy rainfall, and that occurred without significant single triggering factors. A large number of studies have been conducted on landslides induced by strong earthquakes and heavy rainfall. In contrast, landslides like the Zhaobishan SLL, which occurred without strong earthquakes and heavy rainfall, have only gradually attracted much attention from scholars in recent years. Globally, this kind of catastrophic landslides occurs frequently, particularly in certain regions such as the eastern edge of the Tibetan Plateau, the northwestern edge of the Yunnan Plateau, the Rocky Mountains of North America, the Andes of South America, and the European Alps (Delacourt 2004; Handwerger et al. 2013; Lewkowicz and Way 2019; Bontemps et al. 2020). But it is very difficult to understand how the SLL occurs in the absence of heavy rainfall or strong earthquake, and where sufficient water comes from. In addition, SLL often occurs at unexpected times in unexpected places, which significantly increases the difficulty of landslide warning and mitigation. The study of hazards is fundamental in disaster risk science research, and examining the formation mechanism of landslides can improve forecasting capability and the effectiveness of early warning (Alcántara-Ayala et al. 2017; Shi et al. 2020).

Moreover, SLLs are considered an essential process of geomorphic development in mountainous areas (Korup et al. 2007; Egholm et al. 2013; Wang et al. 2020), and the recurring debris flows that result from their occurrence further increase the risk of disaster. From a spatial perspective, the gravitational erosion process in small watersheds in the complex mountainous areas generally originates from large-scale landslides at the source area of the gully and ends in debris flows at the outlet of the gully. The debris flow generation requires sufficient loose material, and landslides are the most common process that supplies these materials in the debris flows of small watersheds (Samodra et al. 2018; Yang et al. 2023). For example, the sources of debris flows typically include landslides, loose deposits in gully beds, moraine deposits, and loess deposits on the eastern edge of the Tibetan Plateau. Among these, moraine deposits are primarily distributed in glacial areas, and weathered loess deposits mainly accumulate on the Loess Plateau areas. Loose deposits in the gully beds are limited to the transportation area. However, the areas mentioned above are relatively small. Therefore, landslides are considered the most common and critical source of debris flows, thereby controlling their frequency and magnitude (Reid et al. 2003; Zhang et al. 2014). For example, in Yunnan Province, China, over 1 million m^3 of landslide source materials are effectively stored in the Jiangjia Gully (48.6 km^2), with the highest frequency of debris flows (approximately 10 events per year) being recorded worldwide (Reid et al. 2003; Zhang et al. 2014). Moreover, in Sichuan Province, China, the pivotal source material of the large-scale debris flow that occurred in Zengda Township on 27 June 2019 was a large-scale rockslide. However, few studies have focused on the formation mechanism and disaster effects of a single SLL that can trigger recurring debris flows in a small watershed.

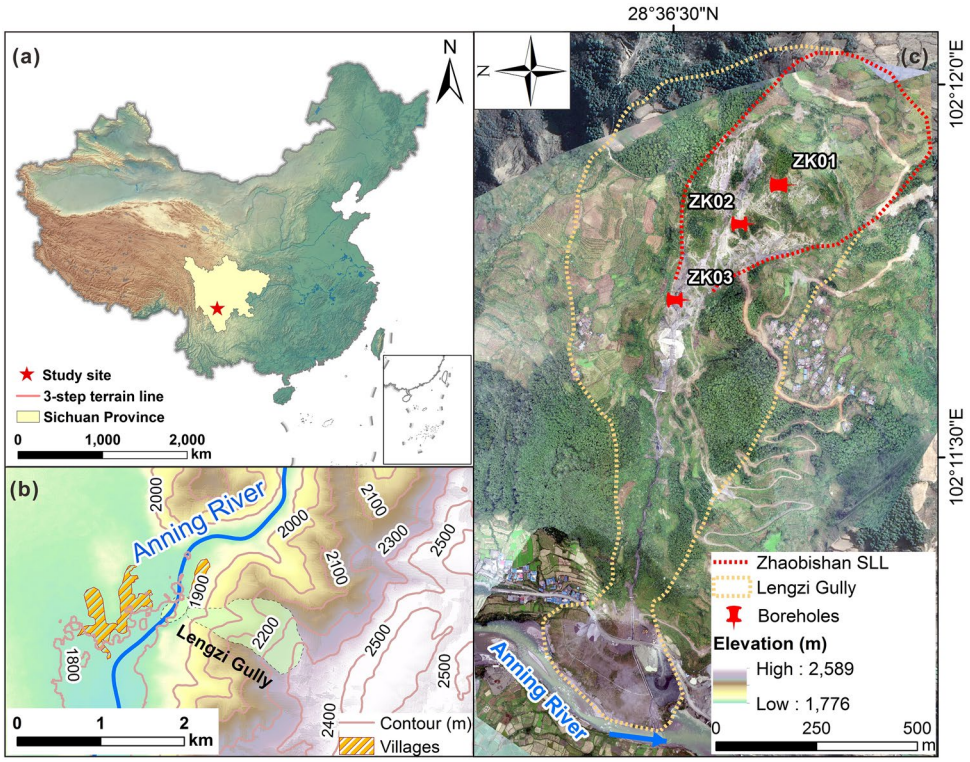

Fig. 1 Location and the geomorphologic features of the Zhaobishan silent large-scale landslide (SLL). **a** The study area in Sichuan Province, China. **b** Topography and settlements of the study area. **c** Orthoimage of the Zhaobishan SLL via unmanned aerial vehicle. ZK01, ZK02, and ZK03 represent the locations of three boreholes with different elevations in the area of the Zhaobishan SLL

Two research problems are addressed in this study: (1) the mechanism of SLL that lags the peak rainfall under non-heavy rainfall and non-seismic conditions; and (2) the characteristics of the debris flow caused by the landslide and its effect in a small watershed. To examine these problems, the Zhaobishan SLL, a rare but typical landslide that has caused ongoing recurring debris flows in the Lengzi Gully, was selected as a case study. First, the Zhaobishan SLL occurred in the inactive period of the Anning River seismic zone (Ni and Song 2019) and was not directly triggered by heavy rainfall or strong earthquakes. In this area, unlike the typical landslide source materials causing debris flow disasters in the watershed following strong earthquakes (Tang et al. 2012; Zhang et al. 2014; Horton et al. 2019), the Zhaobishan SLL is the only single landslide in the basin that continues to trigger recurring debris flows in the Lengzi Gully. Therefore, this study evaluated the mechanism of Zhaobishan SLL and revealed the geological background and hydrological characteristics that facilitate SLLs. The present results provide a new understanding and perspective on the occurrence of SLLs with no strong earthquakes or heavy rainfall, laying a foundation for the risk mitigation of SLLs and associated recurring debris flows in mountainous regions.

2 Materials and Methods

To comprehend the development and failure mechanisms of the Zhaobishan SLL, this study employed a multidisciplinary approach, integrating geology, hydrology, and geotechnics. The methodology encompassed field investigations, hydrological calculations, laboratory experiments, statistical analyses, and numerical simulations. By analyzing the tectonic, geomorphic, and hydrological features of the SLL area, the study aimed to uncover the complex interactions leading to its formation and failure. Notably, the study revealed a time-lagged relationship between landslide deformation and peak rainfall, shedding light on a crucial aspect of the SLL's behavior. Moreover, the investigation focused on the combined influence of weak soil (resulting from fractured rock masses) and intense water flow (due to abundant water infiltration) as drivers for the occurrence of the Zhaobishan SLL.

2.1 Description of the Study Area

The study area is located in Chengxiang Town, Mianning County, Sichuan Province, China (Fig. 1a). The Lengzi

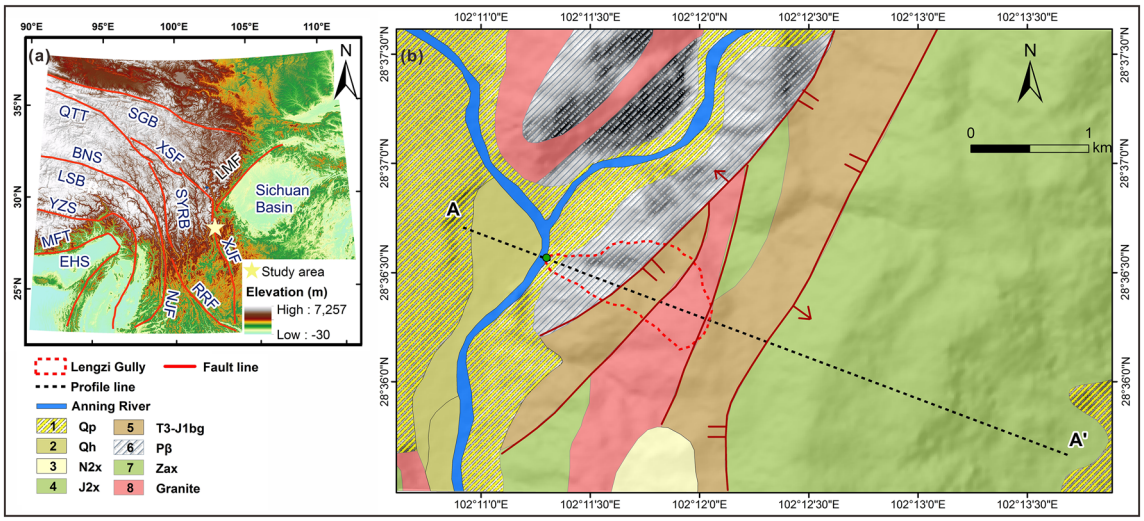

Fig. 2 Geology of the study area. **a** *EHS* Eastern Himalayan syntaxis; *MFT* Main frontal thrust; *YZS* Yarlung-Zangbo suture; *LSB* Lhasa block; *BNS* Bangong-Nujiang suture; *QTT* Qiangtang terrane; *XSF* Xianshuihe fault; *SGB* Songpan-Ganzi block; *LMF* Longmenshan fault; *XJF* Xiaojiang fault; *RRF* Red River fault; *NJF* Nujiang fault; *SYRB* Sichuan-Yunnan rhombic block; **b** AA' is the profile line of Fig. 6b. Q_p and Q_h represent the deposits and alluvial deposits in Quaternary. J_{2x} is the mudstone and siltstone of the Middle Xincun Formation in Jurassic. T_3-J_{1bg} is the feldspar-quartz-sandstone, siltstone, and mudstone intercalated with carbonaceous mudstone of the upper Triassic Baiguowan Group. P_β is the Permian Emeishan basalt. Z_{ax} is the rhyolitic and tuff in the Suxiong Formation of the Lower Sinian System. N_{2x} is the semi-diagenetic clay rocks and siltstone intercalated with fine sandstone of the Xigeda Formation in Tertiary

Gully is a primary tributary on the left bank of the upper reaches of the Anning River (Fig. 1b), and the Zhaobishan SLL is located in the upper reaches of the Lengzi Gully (Fig. 1c). The geographic coordinates at the mouth of the Lengzi Gully are 102°11'23.76" E, 28°36'22.01" N. The Zhaobishan SLL is located in the earthquake zone of the Anning River, which is also a relatively dry zone. The entire study area has a subtropical monsoon climate. The annual temperature varies between 10.3 and 22.6 °C, and the average annual precipitation is between 930 mm and 1210 mm. The study area is dominated by medium and high mountains with steep topography (Ni and Song 2019). In addition, neotectonic movements and precipitation have frequently triggered landslides and debris flows in the study area. From 2000 to 2016, the geohazards in Mianning County have caused 168 casualties and economic losses of USD 80.8 million (Tian et al. 2019). Moreover, the population density in the study area is relatively high (Fig. 1b), and therefore, the SLL and debris flows in the Lengzi Gully directly threaten the lives of 966 people and the safety of USD 52.7 million in assets, including infrastructure such as the Daqiao Hydropower Station and roads.

Tectonically, the study area is located at the edge of the Sichuan-Yunnan rhombic block in the northeastern section of the Hengduan Mountains on the eastern margin of the Tibetan Plateau (Fig. 2a) and belongs to the middle section of the north-south seismic belt in China (Yang et al. 2020). According to the Tibet Autonomous Region Geology and Minerals Bureau (1988), there are three faults from east to west in the study area (Figs. 2 and 5), which pass through the upstream, middle, and downstream reaches of the Lengzi Gully, respectively. The hydrogeological conditions are highly active, and spring water seeps from the slope during our on-site investigation. Lithologically, the rocks comprised of dark gray rhyolitic and tuff in the Suxiong Formation (Z_{ax}) of the Lower Sinian System are exposed at the top area of Zhaobishan SLL, and the rock mass was relatively broken. The Permian Emeishan basalt (P_β) is exposed at the mouth of the Lengzi Gully. Gray-black feldspar–quartz–sandstone, siltstone, and mudstone intercalated with carbonaceous mudstone of the upper Triassic Baiguowan Group (T_3-J_{1bg}) are widely exposed in the study area (Fig. 2). The rocks in the Lengzi Gully vary greatly due to active tectonism. Moreover, there are semi-diagenetic clay rocks and siltstone intercalated with fine sandstone of the Xigeda Formation in Tertiary (N_{2x}) in the upper and middle reaches of the Lengzi Gully.

2.2 Methods

Because landslides are controlled by soil and water conditions (Shoaei and Sidle 2009; Luo et al. 2021), a detailed study of the tectonic setting and hydraulic properties were conducted. Based on the case of the Zhaobishan SLL, the phenomenon and initiation mechanism of SLL were examined through field investigation, meteorological analysis, geological exploration, remote sensing image interpretation, and numerical simulation. The topographic characteristics

were obtained by analyzing the digital elevation model (DEM) data of ALOS-12.5 m DEM and the DEM obtained by unmanned aerial vehicle (UAV) in the study area. Historical insights into the landslide-prone region were acquired through on-site interviews with local residents. During these interviews, a minimum of six local residents were engaged. The questions posed predominantly pertained to the occurrence of past landslides or debris flows in the area, their respective timelines, the severity of the hazards, the depth of mud accumulation, and the distinctive characteristics of the slurry within debris flows, among other aspects. Additionally, our investigation encompassed extensive field work, incorporating activities such as field sampling, cross-section measurements, flow velocity assessments, drone-assisted aerial photography, and an evaluation of land use within the watershed. Characteristic attributes such as the presence of large boulders in the gully were quantified through meticulous measurements as part of our comprehensive survey.

Regarding the tectonic setting, the average fault density index refers to the fault length per unit area (km/km^2), which was obtained by the ArcGIS software in combination with the the geological map of the study area (Tibet Autonomous Region Geology and Minerals Bureau 1988). Based on the data from the United States Geological Survey (USGS) National Earthquake Center (NEIC),[1] we located historical earthquakes from 1900 to the time that the Zhaobishan SLL occurred and set the Zhaobishan SLL as the center with a 420 km search radius. Then the model proposed by Keefer (1984) was used to identify the earthquakes that had an impact on the landslide.

To determine the hydrogeological characteristics of the study area, the Soil Conservation Service Curve Number (SCS-CN) model proposed by the United States Department of Agriculture was used to calculate runoff, and the CN weighted values were determined based on the land use types (Mishra and Singh 2003). The land use types of the study area were obtained by Google Earth image analyses and field investigation. Groundwater characteristics were determined through geological exploration (Fig. 1) and field investigation. Rainfall data were obtained from the meteorological station in Chengxiang Town, which is about 300 m away from the study area.

Based on the geological model of the Zhaobishan SLL derived from the field investigation, the SEEP/W and SLOPE/W modules of the Geo-Studio software were used to analyze the slope instability under the effects of seepage. SEEP/W uses a two-dimensional Richard equation to calculate pore water pressure (PWP). SLOPE/W uses the limit equilibrium method to calculate the factor of safety (Fs) and automatically performs the required Monte Carlo calculation. During the simulation, the PWP values were directly correlated from SEEP/W (Geo-Slope International Ltd. 2007a, 2007b). This method is widely used to simulate landslide stability, particularly in analyzing the instability mechanism of a landslide caused by geotechnical seepage (Chen et al. 2020; Guo et al. 2020). The occurrence of the Zhaobishan SLL was caused by seepage, and this is the reason that we chose this model for our study. Therefore, a finite element model comprising quadrilateral cells and small amounts of trilateral transitional cells was used to study the failure mechanism of the Zhaobishan SLL. The geological profile (Fig. 7 in Sect. 4.2) was selected as the numerical calculation model. The model's length and height were 3,400 and 780 m, respectively. The bottom boundary is the waterproof boundary, and both sides of the model were zero-flow boundaries.

Table 1 Parameters used in numerical studies

Layer	Unit Weight (KN/m^3)	*Ks* (cm/h)	*c* (kPa)	φ (°)
Weathered muddy shale	24.2	0.249	19.9	17.5
Weathered diabase	19.8	0.119	20.0	21.6
Weathered sandstone	25.3	0.250	21.6	19.9
Weathered rhyolite tuff	19.8	0.041	11	36.5

The soil-water characteristic curve (SWCC) was determined by the sample function embedded in the software and the saturated water content. Then, the permeability function was estimated using the Van Genuchten permeability function in SEEP/W. The physical and mechanical parameters of the rock and soil, and their permeability coefficients under saturated conditions (k_s), were determined by field and laboratory experiments. The governing equation in SEEP/W is Richards' equation (Richards 1931), which describes the two-dimensional flow in unsaturated soils, as shown in Eq. (1). The extended Mohr-Coulomb failure envelope (Fredlund et al. 1978) was used to define the shear strength criteria as shown in Eq. (2):

$$\frac{\partial}{\partial x}\left(k_x\frac{\partial h}{\partial x}\right)+\frac{\partial}{\partial y}\left(k_y\frac{\partial h}{\partial y}\right)+Q=\frac{\partial \theta}{\partial t} \tag{1}$$

where x and y are spatial coordinates; θ is the volumetric water content; h is the hydraulic head; k_x and k_y are a function of θ and represent the hydraulic conductivities in the x and y directions, respectively; Q is water flux; and t is time.

$$\tau_f = c\prime + (\sigma - u_a)tan\,\varphi\prime + (u_a - u_w)tan\,\varphi^b \tag{2}$$

where c' is cohesion; φ is the total normal stress on the failure surface; u_a and u_w are net normal stress and matrix potential, respectively; φ' is the internal friction angle

[1] https://earthquake.usgs.gov/earthquakes/search/

Table 2 Historical landslide and debris flow disasters in the study area

Years	Disaster History, Characteristics, and Losses
1920–1930	A landslide occurred in the study area and evolved into multiple debris flows in the Lengzi Gully.
1955	A small-scale collapse occurred on the rear edge of study area.
18 July 2000	The Zhaobishan silent large-scale landslide (SLL) occurred, which is the largest on record and evolved into a debris flow. It caused 1 death, 2 tractors and 4 motorcycles were buried, and the road was buried about 300 m (Sichuan Huadi Construction Engineering Co. Ltd. 2016).
2003, 2007	Large-scale debris flows occurred in the Lengzi Gully, washing out about 450,000 m^3 solid materials, causing the interruption of Road S219, resulting in 1 death, and 3 cars were buried.

related to the net normal stress state variable $(\sigma - u_a)$; and φ^b is the rate at which the shear strength increases with the matrix suction $(u_a - u_w)$.

Additional details can be found in the Emergency Investigation Report of Debris Flows in the Lengzi Gully (Sichuan Huadi Construction Engineering Co. Ltd. 2016) and previous studies (Zienkiewicz and Stagg 1969; Schoeller 1977; Domenico and Schwartz 1998; Weight and Sonderegger 2001), and key parameters of numerical simulation were determined as shown in Table 1. To study the attenuation characteristics of soil strength during the Zhaobishan SLL, the back-analyzed slope stability was conducted. Based on the slope instability conditions, the strength of the soil measured in indoor experiments was reduced until the safety factor of the slope was less than 1.

3 Characteristics of the Zhaobishan Silent Large-Scale Landslide (SLL) and Debris Flows in the Lengzi Gully

On-site interviews and the Emergency Investigation Report of Debris Flows in the Lengzi Gully (Sichuan Huadi Construction Engineering Co. Ltd. 2016) revealed historical evidence that there have been multiple geological disasters in the Lengzi Gully, resulting in severe losses of life and properties (Table 2). According to the records, there have been three landslide events in the Zhaobishan SLL area, which belongs to the upstream portion of the Lengzi Gully. The largest and most recent landslide event occurred on 18 July 2000 and is considered the SLL event in this study. The main sliding direction was 313°, and the volume was about 3.37 million m^3 (Chen et al. 2012). Notably, it was the largest landslide that has occurred so far, and the recurrence interval is approximately 70–80 years in this area. Considering this time scale, the rare large-scale Zhaobishan landslide has led directly to the occurrence of ongoing, high-frequency debris flows in the Lengzi Gully—after the Zhaobishan SLL that occurred on 18 July 2000, debris flows began to occur in the gully in August 2000. Since that time, debris flows have occurred every year in the rainy season, at least once a year, and up to as many as 5–6 per year. To date, debris flow activity has not ceased. Among the debris flow events, the two largest occurred during the rainy seasons in 2003 and 2007.

The Zhaobishan SLL developed in the upper reaches of the Lengzi Gully, and its overall shape was "chair-like." The geographic coordinates at the main scarp of the landslide are 102° 11′ 53.31″ E and 28° 26′ 21.72″ N. The landslide area presents an irregular fan shape in plan view (Fig. 3a), which is conducive to the confluence and runoff. At this stage, the elevation of the steep wall formed by the back cliff of the Zhaobishan SLL is 2195–2290 m a.s.l. (meters above sea level), and the elevation of the shear outlet at the toe of the landslide is approximately 2,030 m a.s.l. To date, the landslide accumulation is 300–570 m long and 160–380 m wide, with an average thickness of approximately 20 m, and a total volume of approximately 270.4×10^4 m^3.

The formation of the Zhaobishan SLL has produced the conditions of high potential sediment yield, strong potential sediment erosion, and high risk of blocking the river. The drainage area of the Lengzi Gully is 0.62 km^2, the length of the main gully is 2 km, and the gully itself presents an overall morphology of gentle slopes in the upstream and downstream sections and steep slopes in the middle section (Fig. 3a). The elevation range of the basin is 1813–2405 m a.s.l., while the relative elevation difference is about 592 m and the average longitudinal slope is 29.6%. With an area of 0.62 km^2, the Lengzi Gully, however, has formed an accumulation fan with an area of 0.1 km^2. Notably, in the Lengzi Gully, the area of the accumulation fan divided by the area of the watershed is 0.16, far exceeding the ratio of 0.01–0.08 in the Xiaojiang Basin and 0.0016–0.29 in the Qiaojia-Menggu section of the Jinsha River Basin (Chen et al. 2005; Liu et al. 2018). On-site investigation of the Lengzi Gully in October 2020 revealed that the original 17 small debris flow check dams in the gully channel were completely silted up (Fig. 3b, c). The average area of a single check dam was about 67.8 m^2, while the average longitudinal slope of the gully bed was 29.6%, so the volume of accumulated silt is estimated to be about 23,000 m^3. These results show that the Lengzi Gully has a high sediment yield and high sediment erosion intensity.

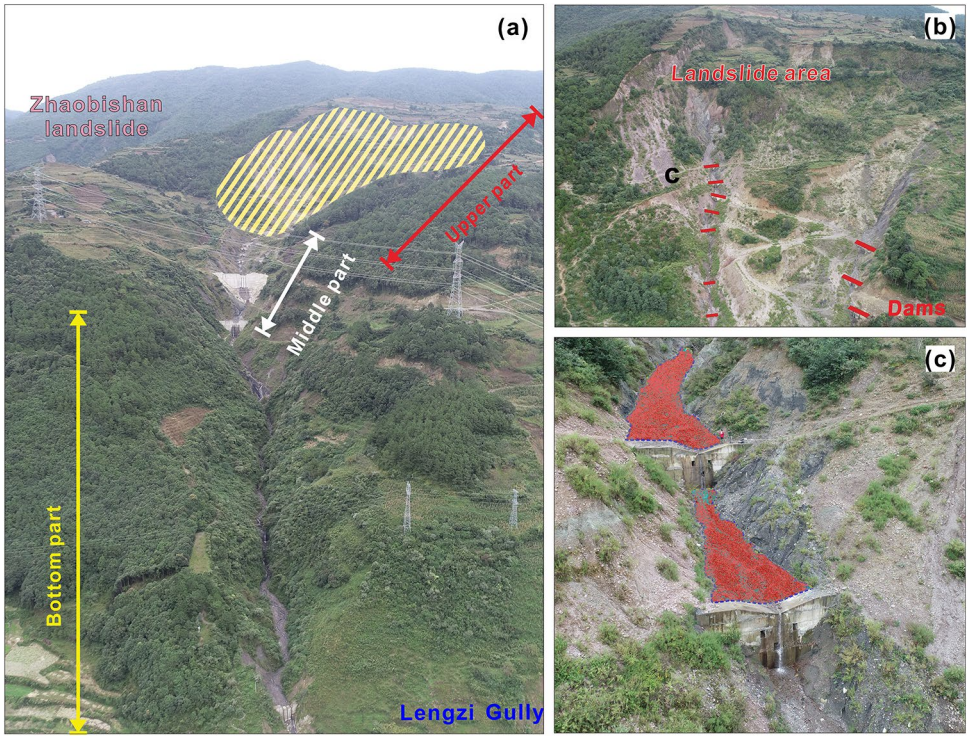

Fig. 3 Landform characteristics of the Zhaobishan silent large-scale landslide (SLL) and the Lengzi Gully. **a** The yellow shaded part represents the area of the Zhaobishan SLL. **b** Red lines indicate the debris flow check dams. **c** Red areas indicate the accumulated silt behind the debris flow check dams

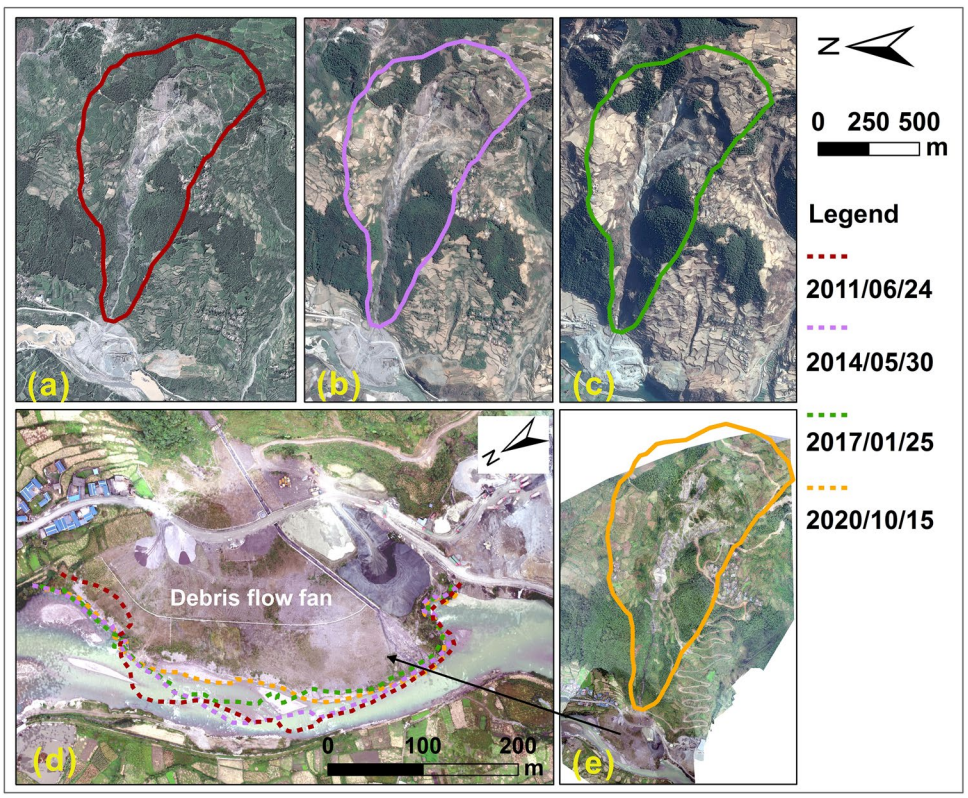

Fig. 4 Remote sensing images of the Lengzi Gully in 2011–2020. Different colors represent the evolution of the Lengzi Gully and the accumulation fan in different years

Due to the extensive accumulation fan of the Lengzi Gully, the Anning River was squeezed to the opposite bank. Multi-phase remote sensing images show that the edge of the debris flow accumulation fan in the Lengzi Gully in 2011 was only 5.9 m away from the right embankment of the Anning River. The distance from the accumulation fan

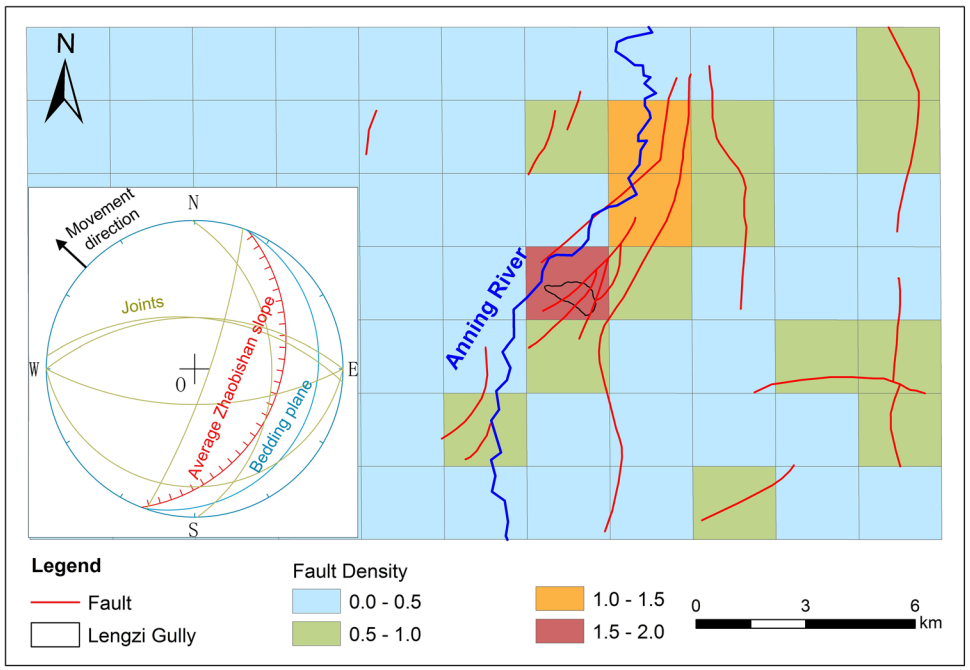

Fig. 5 Fault density of the Zhaobishan landslide silent large-scale landslide (SLL) study area (km/km^2)

to the right embankment in 2014, 2017, and 2020 was 14.1 m, 28.1 m, and 25.2 m, respectively (Fig. 4a–e). Therefore, under the conditions where a large-scale landslide occurs again in the Zhaobishan SLL area, it may further lead to the failure of the debris flow check dams upstream Lengzi Gully and cause severe mass disasters, casualties, and injuries.

4 Results

The broken rock mass developed under active tectonics and strong historical earthquakes had established weak-soil conditions for the Zhaobishan SLL. The combined effect of this distinct lithology, antiform, geomorphic features, and other factors provided favorable conditions for runoff amplification and groundwater seepage and had established strong-water conditions for the Zhaobishan SLL. The coupling effect of strong-water and weak-soil caused by the lagged and enlarged seepage led to a further decrease in rock and soil strength and a further increase in pore water pressure, which ultimately triggered the Zhaobishan SLL.

4.1 Weak-Soil Conditions for the Zhaobishan Silent Large-Scale Landslide (SLL)

Strong tectonic uplifts, high-density faults, and frequent historical strong earthquakes produced fractured rock mass in the slope, thereby leading to the Zhaobishan SLL. The field investigation results show that the slide direction of the Zhaobishan SLL is 313°, and at least six groups of structural planes have developed in the rock mass in the study area (Fig. 5). Among them, the dip of rock mass and two joints in the study area follow the slide direction of the landslide, and the dip of other four joints are oriented from the top to the bottom of the slope on both sides of the Lengzi Gully. As shown in Figs. 8 and 9 in Sect. 4.2, the rock mass of the Zhaobishan SLL is highly fragmented, and the weathering effect is strong; therefore, the slope created weak-soil conditions conducive to landslides occurring.

Existing studies have revealed that the river incision rate of the Anning River in this area from 21 ka BP is 1.63–2.93 mm/y, and the uplift rate from 38 ka BP is approximately 1.9 mm/y (Cheng 2011). Therefore, the entire region is located in a relatively uplifted area, which is conducive to landslides (Ouimet et al. 2007). Second, the average fault density in the Zhaobishan SLL area is relatively high. Studies have revealed that faults control the development of landslides by reducing the strength of rocks and soils. For example, in California, a fault density of 0.093 km/km^2 or above is associated with landslide occurrence (Scheingross et al. 2013); the average fault density in the Parlung Zangbo Basin, where the Yigong landslide occurred, is 0.3 km/km^2. Based on the statistical analysis of this study, the fault density in the Lengzi Gully is 1.625 km/km^2 (Fig. 5), which is considerably higher than in other areas. The high fault density causes strong mutual squeezing between the rock masses, thereby favoring the formation of broken rock mass and weak-soil conditions through additional weathering effect.

Historical strong earthquakes also played a significant role in reducing rock strength and caused the weak-soil condition for the occurrence of the Zhaobishan SLL. However, considering the time scale of the historical earthquakes, they are

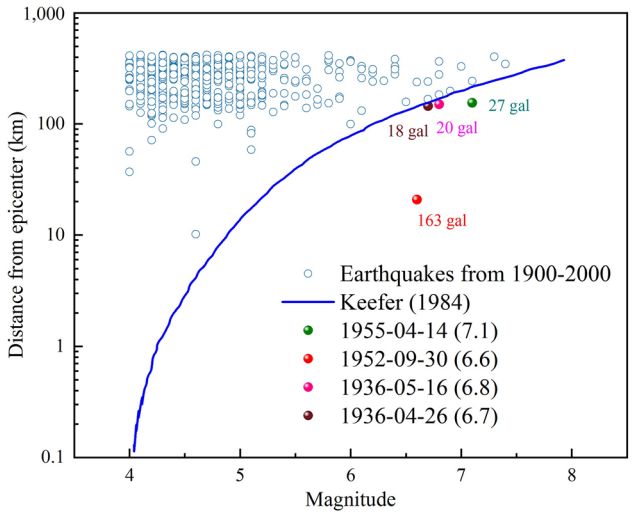

Fig. 6 Influence of earthquakes near the study area (the values within the brackets indicate the magnitude of the respective earthquakes)

study area. Our results show that there were 538 earthquakes with a magnitude greater than Mw 4. According to the empirical model proposed by Keefer (1984), 4 of the 538 earthquakes had a great impact on the stability of the Zhaobishan SLL site (Fig. 6)—the Mw 7.1 earthquake on 14 April 1955, the Mw 6.6 earthquake on 30 September 1952, the Mw 6.8 earthquake on 16 May 1936, and the Mw 6.7 earthquake on 26 April 1936. The last earthquake affecting the Zhaobishan SLL area occurred on 14 April 1955, 45 years before the major landslide in 2000. In addition, according to the seismic acceleration model proposed by Huo and Hu (1992) and Zhou (2019), among the four historical earthquakes having an impact on the stability of the Zhaobishan SLL area, the earthquake in 1952 had considerable seismic influence on the study area, with a seismic acceleration of 163 gal. Although strong historical earthquakes are unlikely a direct triggering factor of the Zhaobishan SLL, such earthquakes are conducive to the fragmentation and weathering of the original intact rock mass and formation of the weak-soil conditions.

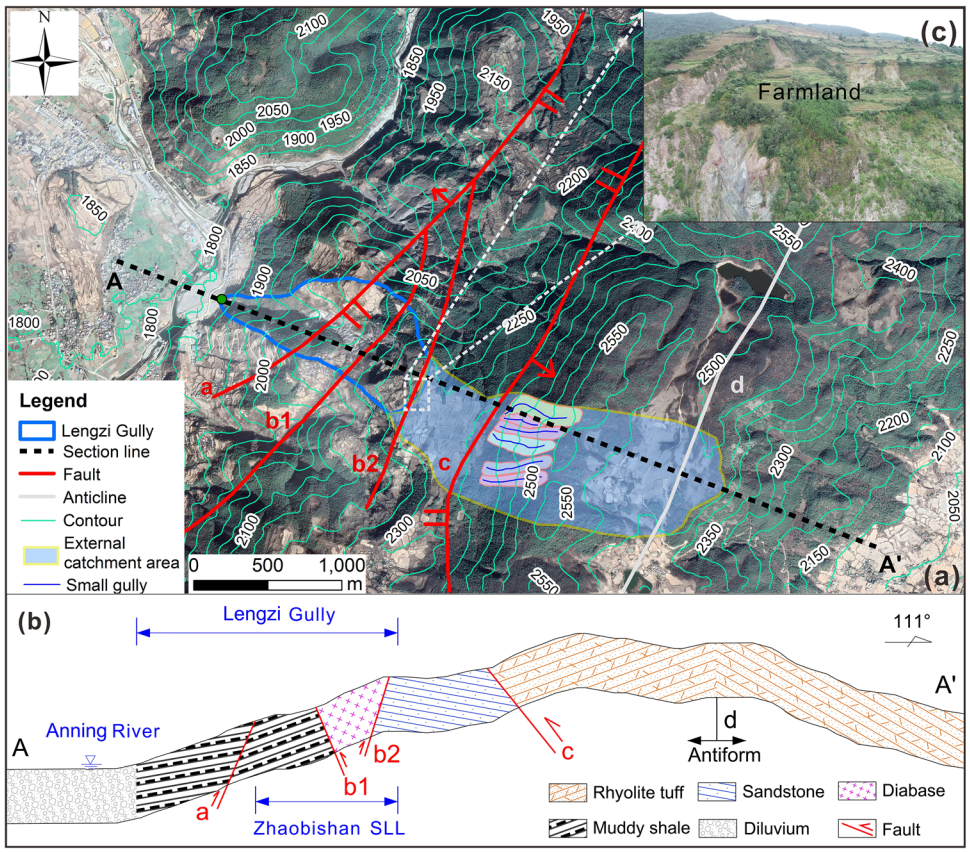

Fig. 7 Geomorphic and geological characteristics of the Zhaobishan silent large-scale landslide (SLL) study area. **a** Topographic map in plan view showing structural geological features. **b** Geological profile map showing four identified faults and the antiform. **c** Image of the present-day farmland on the top of the slope

unlikely a direct triggering factor for the Zhaobishan SLL. Stronger earthquakes have a significant impact on landslides. For example, studies have revealed that the impact distance of an earthquake of moment magnitude (Mw) 8 on landslides is approximately 418.5 km (Keefer 1984); however, there have been no recent earthquakes with such a high magnitude in the

4.2 Strong-Water Conditions for the Zhaobishan Silent Large-Scale Landslide (SLL)

The combined effect of unique lithology, antiform, large water confluence area, and cultivated land provided

favorable runoff and groundwater seepage conditions. The geological profile AA' shows that one antiform structure (Fig. 7; structure marked as d) and four faults (Fig. 7; faults marked as a, b1, b2, and c) have developed from east to west. The antiform d on the hanging wall of fault c formed in the rhyolite and tuff of the Lower Sinian system. The stratum on the side close to the landslide is leaning toward the landslide at 291°, and the stratum on the other side is leaning at 111°. Reasonably, the antiform, which comprises a mountainous feature, is a watershed dominated by groundwater. In addition, field investigation and remote sensing images revealed that the core of the mountain with the antiform has experienced severe weathering. Furthermore, a farmland platform with a length of approximately 1.5 km appears in the core area on the profile with the section line AA'. Such a platform topography provides favorable conditions for runoff. The sandstone of the late Triassic Baiguowan Group, with well-developed joints and fissures and good permeability, developed between faults b2 and c. The block area between faults b1 and b2 formed from diorite intrusive in the early Triassic, with well-developed joints and strong permeability. In addition, the block area is surrounded by sandstone and shale of the Baiguowan Group, and the elevation of the block area between faults b1 and b2 is relatively high. Therefore, the block area between faults b1 and b2 is determined by the hanging wall of faults b1 and b2. In addition, strongly weathered shale of the Baiguowan Group was developed between faults a and b1.

The internal dynamic compression of multiple faults and the antiform led to broken rock masses inside the slope. Subsequently, under external forces such as weathering and anthropogenic activities, platform water storage area was formed in the core of the antiform. Moreover, highly permeable lithology, such as the sandstone and broken rock mass, provides good seepage conditions to replenish the groundwater in the study area.

The confluence area of long-distance water replenishment outside the Zhaobishan SLL body is 3.16 times the area of the slope body. Field investigation and remote sensing images revealed that the shear outlet elevation of the Zhaobishan SLL is located at approximately 2,030 m a.s.l. Above the outlet elevation, the catchment area of the Zhaobishan SLL is only 0.44 km^2. However, the total water-replenished confluence area at the back of the slope is 1.39 km^2, of which only 0.5 km^2 is covered by vegetation, and the remaining 0.89 km^2 is bare farmland (Fig. 7c). In addition, there are six small gullies developed at the top of the slope (Fig. 7a), with total areas of 46,586, 22,400, 32,768, 54,443, 50,628, and 57,643 m^2 from north to south, and a cumulative total area of approximately 0.26 km^2. The development of such small gullies also contributed to the runoff to the landslide body.

Field investigation and geological exploration found 11 springs exposed on the slope of the Zhaobishan SLL at the locations described in Table 3, and their elevation range is between 2011 and 2142 m a.s.l. The spring with the highest altitude is located at the back edge of the landslide body with an elevation of about 2142 m a.s.l. The spring with the lowest altitude is situated at the forefront of the landslide mass, positioned at an elevation of approximately 2011 m a.s.l. In addition, field investigations and remote sensing images show three belt-like permeable layers in the upper reaches of the Lengzi Gully (Fig. 8), with thicknesses ranging from 0.58 to 1.12 m.

Table 3 The characteristics of springs exposed during the field investigation

ID	Elevation (m)	Discharge (L/s)	ID	Elevation (m)	Discharge (L/s)
1	2142	0.03	7	2075	0.14
2	2140	2.00	8	2065	0.09
3	2103	9.72	9	2050	0.05
4	2088	2.10	10	2035	0.06
5	2088	0.11	11	2011	0.01
6	2075	2.50			

Core analysis from the three boreholes ZK01, ZK02, and ZK03 revealed that most of the Zhaobishan SLL deposits are on the upper, middle, and lower parts of the upstream reach of the Lengzi Gully. Borehole ZK01 revealed that the thickness of the landslide deposits distributed on the upper part is approximately 46.5 m, accumulated on the broken tuff of the Suxiong Formation in the Sinian System. Borehole ZK02 revealed that the thickness of the landslide deposits distributed in the middle part is approximately 20.4 m, accumulated on the 4.6 m thick semi-diagenetic clay rock of the Xigeda Formation in the Tertiary System and gray diorite of the Lower Proterozoic. Borehole ZK03 revealed that the thickness of the landslide deposits distributed in the lower part is approximately 12.9 m, accumulated on the 5.2 m thick semi-diagenetic clay rock of the Xigeda Formation and carbonaceous shale of the Baiguowan Formation in the Triassic System. Importantly, ZK02 and ZK03 revealed that the groundwater level is in a belt-shaped zone of 10.9–19.0 m from the surface. The histogram and borehole profiles are shown in Fig. 9. The field investigation also revealed that the Zhaobishan SLL was in a state of continuous creep, and many cracks had gradually formed behind the main scarp of the landslide. Based on the on-site interviews with the local residents, before the Zhaobishan SLL event in 2000, the current shear outlet area at the front edge of the slope was a natural slope landform, and spring water was exposed, which was the source of the water flow in the Lengzi Gully.

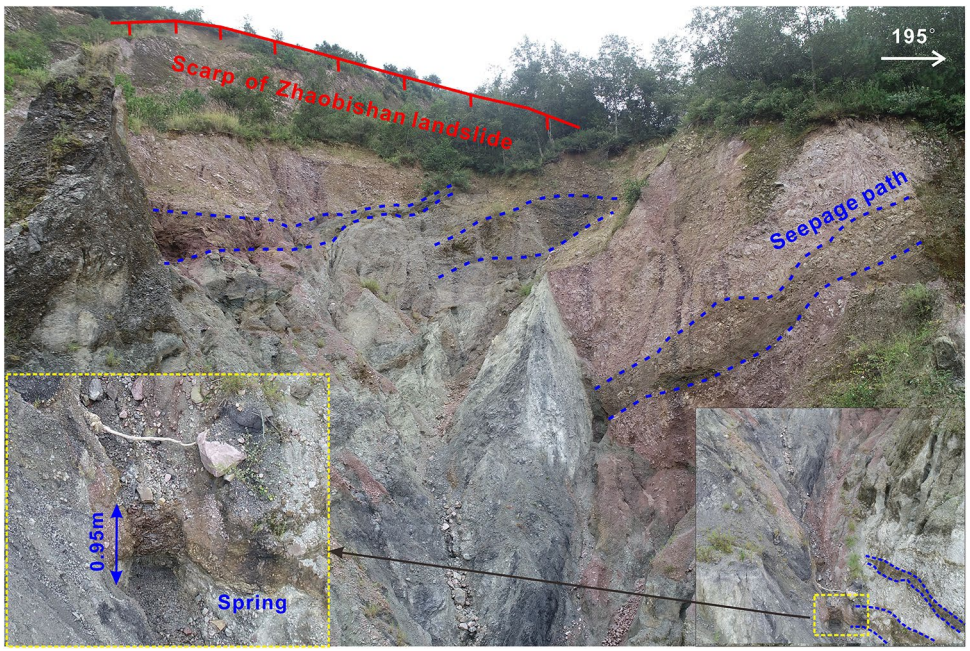

Fig. 8 Groundwater characteristics of the Zhaobishan silent large-scale landslide (SLL) at the source area of the Lengzi Gully

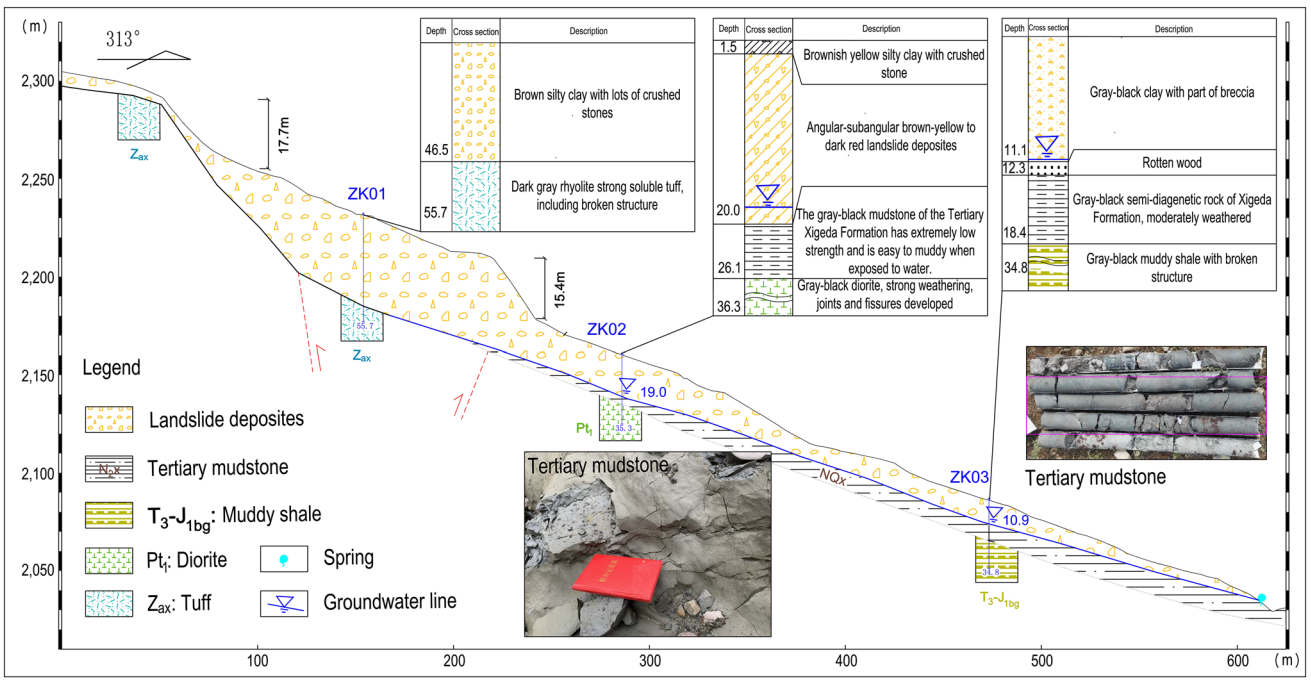

Fig. 9 Geological profile and histogram of the Zhaobishan silent large-scale landslide (SLL). Source Sichuan Huadi Construction Engineering Co. Ltd. (2016)

4.3 Water-Soil Coupling Triggering Effect of the Zhaobishan Silent Large-Scale Landslide (SLL)

The large water confluence area and long-distance groundwater replenishment behind the main scarp of the slope provided abundant water source conditions and directly led to the occurrence of the Zhaobishan SLL. The occurrence time lagged the peak rainfall by 4.6 days. By analyzing the geological and hydrogeological characteristics of the study area, the area of the Zhaobishan SLL was 0.44 km^2. However, the confluence area that can provide water replenishment for the seepage of the Zhaobishan SLL was 1.39 km^2, including 0.69 km^2 on the front side and 0.7 km^2 on the backside of

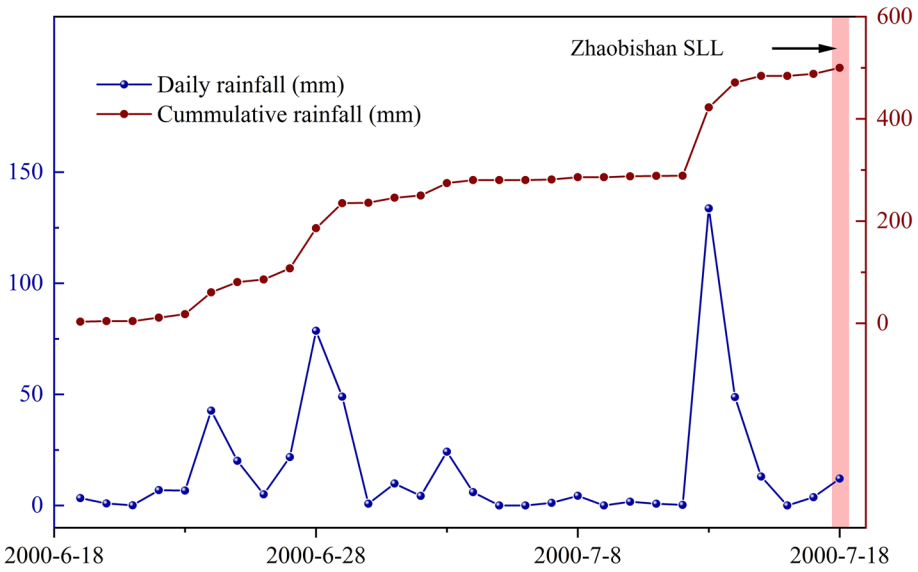

Fig. 10 Rainfall characteristics before the Zhaobishan silent large-scale landslide (SLL) showing the occurrence time of the landslide lagging the peak rainfall by approximately 5 days

the slope. Evidently, 0.47 km^2 of the seepage replenishment area on the front side of the slope was covered by farmland, accounting for 68.1% of the total seepage replenishment area on the front side of the slope. In addition, 0.42 km^2 of the seepage replenishment area on the backside of the slope was also covered by farmland, accounting for 60.0% of the total seepage replenishment area on the backside of the slope. According to these characteristics and the SCS-CN model (Mishra and Singh 2003), runoff was calculated, and the CN weighted values for the areas in the front and back of the slope were 52.8 and 61.0, respectively. The hydrological calculations revealed that, under the maximum daily rainfall of 133.7 mm, the runoff depths at the front and back of the slope are 24.7 and 38.87 mm, respectively. This shows that 81.6% and 70.9% (respectively) of the runoff is involved in the infiltration process. The results also show that considering the large area of runoff and long-distance groundwater replenishment, the seepage amount in the landslide area is 3.95 times that only considering the landslide body. In addition, based on Google Earth image analyses and the findings of the geological exploration, the total length of the groundwater seepage path from the back-shaped mountain on the backside of the slope to the locked section of the Zhaobishan SLL is estimated to be approximately 2.5 km.

The peak rainfall in the early stage sharply increased the seepage amount in the landslide area, and finally, the coupling effect of strong-water and weak-soil triggered the Zhaobishan SLL in 2000. According to the data from the meteorological station in Chengxiang Town, there was only 12.1 mm of rainfall on the day of the landslide. Such a low rainfall intensity is unlikely to cause large-scale landslide disasters. However, on 13 July 2000, the total daily rainfall in the study area was 133.7 mm, with a recurrence interval of 20 years. Approximately 5 days later, at 8 a.m. on 18 July, the Zhaobishan SLL occurred (Fig. 10). Therefore, the Zhaobishan SLL lagged approximately 5 days than the peak rainfall in the time sequence. This lag is typical of SLL events, which often makes the prediction and early warning of this type of landslide extremely arduous. Therefore, rainfall, particularly the continuous antecedent rainfall, is a crucial factor that can induce aggravated deformation of landslides and trigger the failure of the slope (Tian et al. 2020a).

The results from the computation model of Zhaobishan SLL (Fig. 11) show that under the combined effect of seepage replenishment on the front side and backside of the slope, the occurrence time of the Zhaobishan SLL lagged the peak rainfall by 4.6 days (Fig. 10). Also, the model outputs were validated by comparison with groundwater levels in the boreholes, the outlets location of the springs recorded during on-site investigation and on-site interviews. Therefore, the process of regional precipitation→runoff→long-distance water replenishment→soil-water interaction→strength reduction→landslide requires approximately 4.6 days in the Zhaobishan SLL area. This long-chain process is the key factor for the lagging time between the occurrence time of landslides and peak rainfall. The results from SLOPE/W based on SEEP/W show that the increase in pore water pressure and the attenuation of the rock and soil strength together triggered the Zhaobishan SLL. Based on the slope instability conditions, the back-analyzed slope stability reveals that the pore water pressure at the monitoring points in the slope increased from the initial -14.95 kPa to 311.29 kPa within 4.6 days. The strength of highly weathered shale and diabase was reduced to 0.39 times and 0.38 times of the initial rock strength, respectively. Eventually, the safety factor of the slope was reduced to 0.99, and the Zhaobishan SLL occurred (Fig. 12).

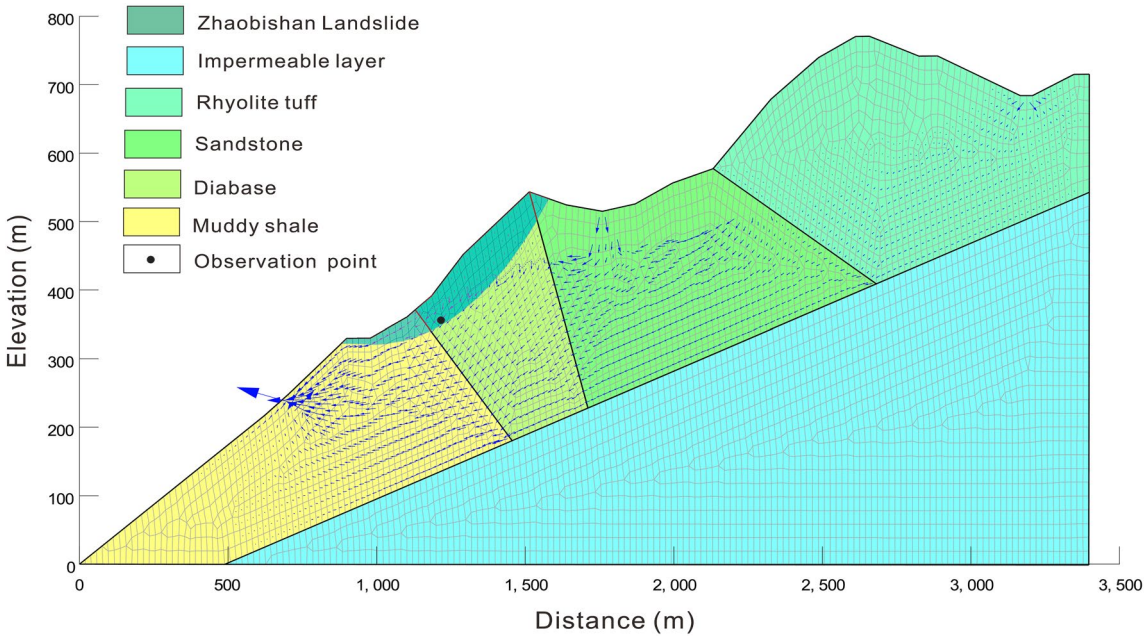

Fig. 11 Computation model of the Zhaobishan silent large-scale landslide (SLL) in Geo-studio

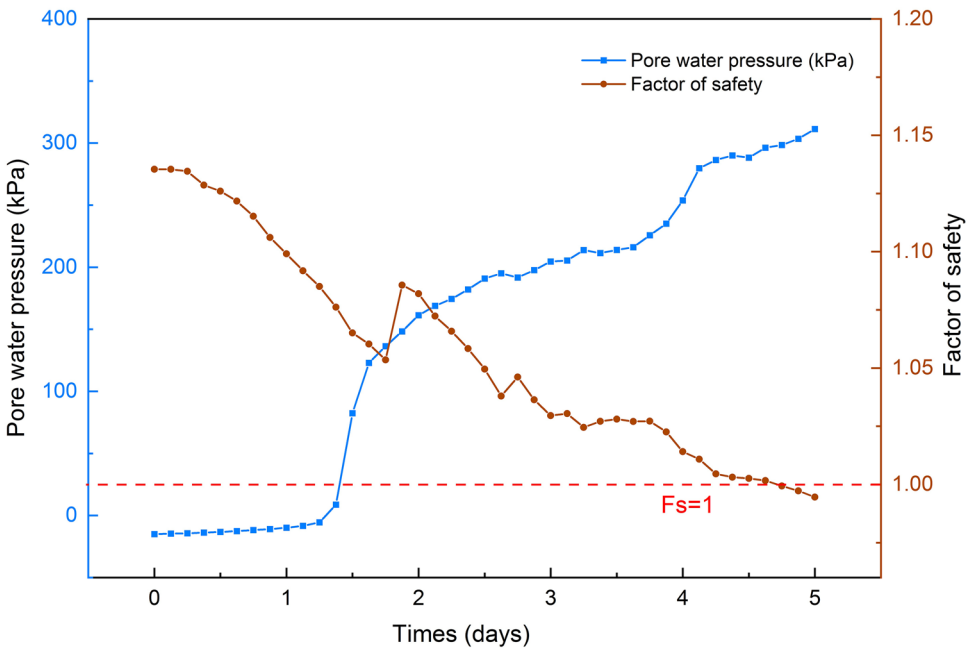

Fig. 12 Variation trend of the safety factor and pore water pressure of the observation point through numerical simulation

5 Discussion

The strata of the Xigeda Formation (Nqx) play a significant role in the transition of landslides into debris flows within smaller watersheds, thereby exacerbating the level of disaster risk. Furthermore, the destabilization mechanism outlined in this study for the Zhaobishan SLL differs from landslides triggered by intense seismic activity or heavy precipitation. Instead, the primary driver is the heightened runoff resulting from dynamic tectonic processes and intricate hydrological conditions. This distinction underscores the importance of early identification of such landslides based on the hydrological and geological characteristics of the SLL area, and highlights the necessity of accounting for the delayed peak rainfall patterns in monitoring and issuing timely warnings as part of future SLL risk management strategies.

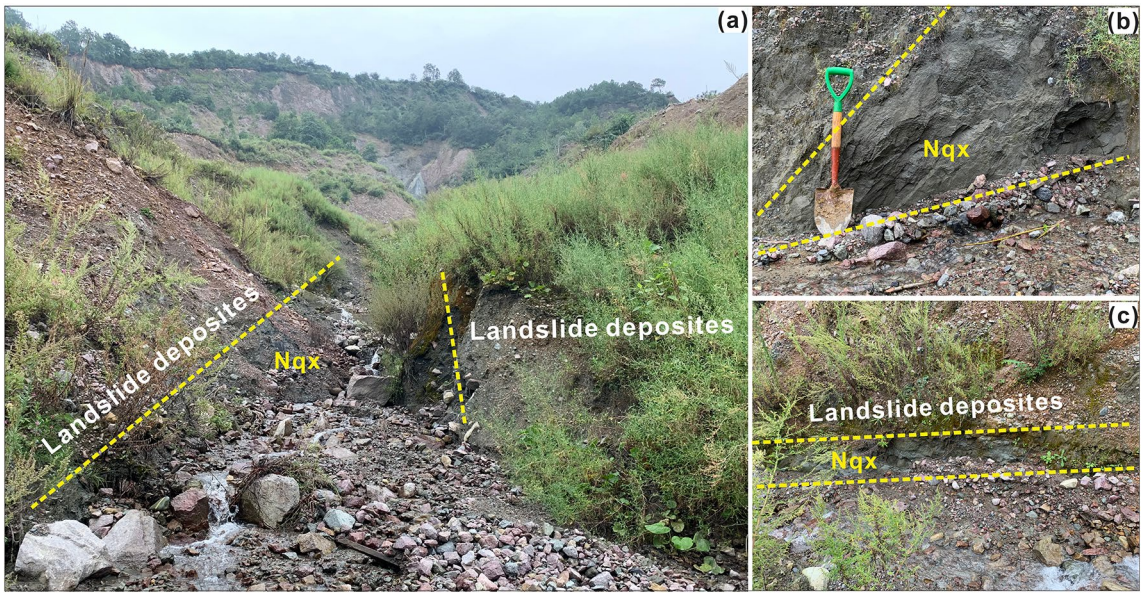

Fig. 13 Deposits of the Zhaobishan silent large-scale landslide (SLL) accumulated on the semi-diagenetic clay rocks (Nqx)

5.1 Increased Risk of Zhaobishan Silent Large-Scale Landslide (SLL) Transforming into Debris Flows

Regional multi-hazard and disaster chains can amplify hazard intensity and change the scope of affected areas (Shi et al. 2020). The transformation of the Zhaobishan SLL into multiple large-scale debris flows has expanded the scope of affected areas and lengthened the duration of the disaster impact. After the Zhaobishan SLL in 2000, no large-scale landslide has occurred in the Lengzi Gully until 31 December 2022, but several debris flows have occurred, forming a large deposit fan with an area of 0.1 km^2, causing considerable social, economic, and ecological losses and seriously threatening local residents, the Anning River, and the hydropower station. Based on the combined analyses, after the Zhaobishan SLL in 2000, the strata of the Xigeda Formation (Nqx), which are distributed in the Lengzi Gully, controlled the formation of a new seepage system in the slope. There are generally two models for transforming a landslide into a debris flow. The first is that the landslide is transformed into a debris flow and directly converted into subsequent multiple debris flows under rainfall or runoff. For example, the Yigong landslide that occurred on 9 April 2000 at the eastern edge of the Tibetan Plateau led to a considerable debris flow in the Zamunong Gully (Delaney and Evans 2015). The second is that a small part of the landslide deposit directly participates in the debris flow. Most deposits are accumulated on the slope surface, and thus, further erosion will be triggered on a longer time scale under the influence of rainfall or runoff. An exceptional phenomenon associated with the second model of landslides can describe the Zhaobishan SLL and Lengzi Gully debris flows involved in this study. The field investigation revealed that the semi-diagenetic clay rocks of the Xigeda Formation in the Tertiary System were exposed at the Lengzi Gully (Fig. 13). After the Zhaobishan SLL in 2000, most deposits were accumulated on the original semi-diagenetic clay rocks upstream of the Lengzi Gully. Here, the semi-diagenetic clay rock with poor water permeability served as the aquiclude. Thus, a new groundwater boundary condition was created between the overlying landslide deposits and the stratum of the Xigeda Formation. In this new seepage system, the carbonaceous semi-diagenetic clay rock was prone to local slumping after being softened by water, which likely played a role in reducing the rainfall threshold required for landslides and debris flows (Xu and Liu 2011). Therefore, the landslide deposits of the Zhaobishan SLL could easily participate in multiple debris flow events in the Lengzi Gully over a longer time because the critical rainfall intensity was not very high. Moreover, based on the situation that the Zhaobishan SLL was at risk of further sliding, it is necessary to conduct detailed monitoring work in the area.

5.2 Failure Mechanism Comparing to Other Types of Landslides

The water-soil interaction was well known as a necessary condition for landslides, but there are differences in the formation mechanisms of different landslides. First, for the coseismic landslides or strong earthquake-triggered landslides, researchers studied their mechanism by analyzing detailed coseismic landslide inventories after strong

earthquakes (Gorum et al. 2011; Tanyas et al. 2017) or by numerical simulations and shaking table tests (Podolskiy et al. 2015; Jibson 2011). The response of the slope to earthquakes mainly includes the reduction of elastic modulus, the formation or widening of cracks at the top of the slope, and the generation of excess pore water pressure, which further leads to the reduction of the soil strength and the occurrence of coseismic landslides (Wang et al. 2001; Rivière et al. 2015; Fan et al. 2019). Second, regarding the rainstorm-induced landslides or heavy rainfall-induced landslides (often associated with extreme rainstorms triggered by typhoons), the infiltration of rainwater from landslide areas leads to the increase of soil water content, pore water pressure, and buoyancy force, the formation of the saturated sliding surface, the decrease of soil strength, and finally, the occurrence of landslides (Xu et al. 2016; Wu et al. 2017; Wang et al. 2019). The erosion of river banks by floods formed by heavy rainfall can also lead to slope failure (Chen et al. 2014). Third, the mechanism of the landslide examined in this study, that is, weak-soil and strong-water jointly controlling the occurrence of SLL under the active tectonic and complex hydrological background, is consistent with existing studies. For example, studies have found that the coupling of small to medium earthquakes and hydrological conditions is conducive to the occurrence of landslides (Bontemps et al. 2020). Ambrosi and Crosta (2006) pointed out that tectonic, lithology, groundwater fluctuations, and weathering effects significantly impact large landslides in the central Italian Alps. Therefore, strong earthquake-induced landslides and heavy rainfall-induced landslides are directly triggered by strong earthquakes or heavy rainfall; SLLs, on the other hand, are caused by the amplified seepage under the active tectonic and complicated hydrological conditions.

5.3 Characteristics and Control Strategy of Risks Induced by Silent Large-Scale Landslides (SLL)

To reduce the disaster risk of SLL hazards, we summarize the spatial and temporal characteristics and discuss the risk-control strategy of SLL based on the results of our field investigation, numerical simulation, and other existing studies.

First, the timing of SLLs is often unexpected because they are not directly triggered by heavy rainfall or strong earthquakes. The timing of SLLs is different from conventional landslides, and the unexpected timing increases the disaster risk of landslide hazards. For example, the 2018 Baige SLL along the Jinsha River in Tibet occurred in late October and early November, which is not the rainy season, and there was no obvious rainfall process when it occurred (Deng et al. 2019). Although the 2017 Xinmo SLL in Maoxian, Sichuan Province in China occurred in June, there was no obvious rainfall process when it occurred, and the daily rainfall on the day of the landslide was only 2–5 mm (Xu et al. 2017). In this study, the Zhaobishan SLL and the previous peak rainfall also showed time-lagging characteristics. The large water confluence area behind the main scarp of the landslide and the lag of amplified runoff determined the delayed occurrence of the landslide. Therefore, the initiation mechanism of SLL proposed here may be used to explain the hysteresis phenomenon between landslides and peak rainfall. To mitigate the disaster risks of SLL, special attention should be paid to the hysteresis characteristics between the time of potential landslides and peak rainfall to improve the early warning system. Awareness of local residents also should be enhanced through education and training. In addition, the prediction of these landslides should not be conducted solely based on rainfall intensity, and vigilance against landslides and deformation monitoring must be increased after heavy rainfall.

Second, the location of SLLs has special characteristics because these landslides are jointly controlled by weak-soil (fractured rock mass) and strong-water (abundant water replenishment) conditions under the impact of active tectonism and complex hydraulic properties. For example, the water confluence area behind the main scarp of the Zhaobishan SLL is 3.16 times the area of the slope body. Water in the Bogong Gully, with a catchment area of 23.2 km^2, behind the main scarp of the Baige landslide, refilled the long-term seepage within the slope of the Baige landslide (Tian et al. 2020a, b). Similarly, on 25 April 1974, the Mantaro landslide in Peru occurred because of the increased seepage caused by the infiltration of the Pumaranra River behind the slope (Berrocal et al. 1978). Therefore, SLLs usually occur on slopes with strong tectonic uplifts, high-density faults, frequent historical strong earthquakes, and large water confluence areas behind the main scarp. These characteristics help enhance the accuracy of SLL identification, which is crucial for landslide warning and disaster risk reduction. Consequently, we also need to pay attention to the following aspects in the mitigation of disaster risk: (1) the long-distance groundwater replenishment in the slopes should be considered in the prediction and warning of landslides; (2) the impact of geological and geomorphic features on the runoff and groundwater seepage should be analyzed during the early identification of landslides; and (3) remote sensing images should be used to analyze land use conditions, and special attention should be paid to the water confluence and infiltration from farmland.

Finally, for the watersheds with semi-diagenetic clay rocks of the Xigeda Formation, recurring debris flows following massive landslides also should be focused, and high-efficiency sediment drainage should be conducted to avoid the outburst floods caused by the blockage of the main river.

5.4 Limitation

There has been increasingly more attention to SLL and some studies reported that tectonic activity and groundwater play an essential role in the occurrence of landslides and debris flows (Wei et al. 2019; Bontemps et al. 2020), which is largely consistent with our results. However, the mechanism through which the amplified runoff affects the rock mass strength after infiltration, quantification of the influence of tectonic activity on landslides, and physical process of transforming rare landslides into recurring debris flows, are all topics necessitating further research.

6 Conclusion

Taking the Zhaobishan SLL, that has been causing recurring debris flows since 2000 in the Lengzi Gully on the eastern edge of the Tibetan Plateau, as a case study, the coupling effect of weak-soil (fractured rock mass) and strong-water (abundant water replenishment) on the occurrence of SLL was revealed through field investigation, remote sensing image analysis, geological exploration, hydrological calculation, and numerical simulation. The results explain why SLL lags the peak rainfall and provide new insights into the risk mitigation of these distinct landslides and debris flows in vulnerable mountainous areas.

The Zhaobishan SLL was associated with high sediment yield, substantial sediment erosion, and high risk of river blocking in the Lengzi Gully. Strong tectonic uplift, high fault density, and multiple historical strong earthquakes had established weak-soil conditions, and the combined effect of special lithology, antiform, large regional water confluence area, and cultivated land had established strong-water conditions, which are both conducive to the occurrence of the landslide. Extensive runoff and long-distance water replenishment created the instability and lagging effect of the Zhaobishan SLL. The coupling effect of strong-water and weak-soil on the slope body eventually attenuated the rock and soil strength to approximately 0.4 times its initial strength, triggering the landslide. The Zhaobishan SLL combined with the exceptional setting of semi-diagenetic clay rocks of the Xigeda Formation also contributed to the recurring debris flows in the Lengzi Gully. To reduce disaster risk of SLL in vulnerable mountainous areas, the water confluence area behind the main scarp of landslides, the hysteresis characteristics between the landslides and peak rainfall, and the long-distance water replenishment of slopes should be further considered, and recurring debris flows following massive landslides also should be focused.

Acknowledgments This study was financially supported by the National Natural Science Foundation of China (Grant No. U20A20110), the Second Tibetan Plateau Scientific Expedition and Research Program (STEP) of China (Grant No. 2019QZKK0902), the Youth Innovation Promotion Association CAS (ID 2020367), and the International Cooperation Overseas Platform Project, Chinese Academy of Sciences (Grant No. 131C11KYSB20200033). All financial supports are greatly appreciated. The authors would like to thank the Sichuan Huadi Construction Engineering Co. Ltd. and Liangshan Meteorological Office for their data and help.

References

Alcántara-Ayala, I., K. Sassa, M. Mikoš, Q. Han, J. Rhyner, K. Takare, S. Nishikawa, B. Rouhban, and S. Briceno. 2017. The 4th world landslide forum: landslide research and risk reduction for advancing the culture of living with natural hazards. *International Journal of Disaster Risk Science* 8(4): 498–502.

Ambrosi, C., and G.B. Crosta. 2006. Large sackung along major tectonic features in the central Italian alps. *Engineering Geology* 83: 183–200.

Bahrami, S., B. Rahimzadeh, and S. Khaleghi. 2019. Analyzing the effects of tectonic and lithology on the occurrence of landslide along Zagros ophiolitic suture: A case study of Sarv-Abad, Kurdistan. *Iran. Bulletin of Engineering Geology and the Environment* 79: 1619–1637.

Berrocal, J., A.F. Espinosa, and J. Galdos. 1978. Seismological and geological aspects of the Mantaro landslide in Peru. *Nature* 275: 533–536.

Bontemps, N., P. Lacroix, E. Larose, J. Jara, and E. Taipe. 2020. Rain and small earthquakes maintain a slow-moving landslide in a persistent critical state. *Nature Communications* 11: Article 780.

Carlini, M., A. Chelli, R. Francese, S. Giacomelli, M. Giorgi, A. Quagliarini, A. Carpena, and C. Tellini. 2017. Landslides types controlled by tectonics-induced evolution of valley slopes (Northern Apennines, Italy). *Landslides* 15: 283–296.

Carlini, M., A. Chelli, P. Vescovi, A. Artoni, L. Clemenzi, C. Tellini, and L. Torelli. 2016. Tectonic control on the development and distribution of large landslides in the Northern Apennines (Italy). *Geomorphology* 253: 425–437.

Chen, S., H. Chou, S. Chen, C. Wu, and B. Lin. 2014. Characteristics of rainfall-induced landslides in Miocene formations: a case study of the Shenmu watershed, Central Taiwan. *Engineering Geology* 169: 133–146.

Chen, Y.-L., G.-Y. Liu, N. Li, X. Du, S.-R. Wang, and R. Azzam. 2020. Stability evaluation of slope subjected to seismic effect combined with consequent rainfall. *Engineering Geology* 266: Article 105461.

Chen, J., F. Wei, and P. Cui. 2005. Restricting conditions and their characteristics for debris flow fans in Xiaojiang River Valley. *Scientia Geographica Sinica* 25: 704–708 (in Chinese).

Chen, X., Y. You, X. Chen, J. Liu, and K. Huang. 2012. Characteristics and development trends of debris flows of Lengzi Gully in the upper Anning River, southwest Sichuan, China. *Resource and Environment in the Yangtze Basin* 21: 122–128 (in Chinese).

Cheng, J. 2011. Evolution of terraces I-III along the Anning River, western Sichuan, based on pollen records and terrace structure. *Science China Earth Sciences* 54: 127–135.

Delacourt, C. 2004. Velocity field of the "La Clapière" landslide measured by the correlation of aerial and quickbird satellite images. *Geophysical Research Letters*. https://doi.org/10.1029/2004GL020193.

Delaney, K.B., and S.G. Evans. 2015. The 2000 Yigong landslide (Tibetan Plateau), rockslide-dammed lake and outburst flood: Review, remote sensing analysis, and process modelling. *Geomorphology* 246: 377–393.

Deng, J., Y. Gao, Z. Yu, and H. Xie. 2019. Analysis on the formation mechanism and process of Baige landslides damming the upper reach of Jinsha River, China. *Advanced Engineering Sciences* 51: 9–16 (in Chinese).

Domenico, P.A., and F.W. Schwartz. 1998. *Physical and chemical hydrogeology*. New York: John Wiley and Sons.

Egholm, D.L., M.F. Knudsen, and M. Sandiford. 2013. Lifespan of mountain ranges scaled by feedbacks between landsliding and erosion by rivers. *Nature* 498: 475–478.

Evans. 2011. *Natural and artificial rockslide dams*. Berlin: Springer.

Fan, X., C.H. Juang, J. Wasowski, R. Huang, Q. Xu, G. Scaringi, C.J. van Westen, and H.-B. Havenith. 2018. What we have learned from the 2008 Wenchuan Earthquake and its aftermath: A decade of research and challenges. *Engineering Geology* 241: 25–32.

Fan, X., G. Scaringi, O. Korup, A.J. West, C.J. van Westen, H. Tanyas, N. Hovius, and T.C. Hales et al. 2019. Earthquake induced chains of geologic hazards: Patterns, mechanisms, and impacts. *Reviews of Geophysics*. https://doi.org/10.1029/2018RG000626.

Fredlund, D.G., N.R. Morgenstern, and R.A. Widger. 1978. The shear strength of unsaturated soils. *Canadian Geotechnical Journal* 15(3): 313–321.

Geo-Slope International Ltd. 2007a. SEEP/W user's guide for finite element seepage analysis. Calgary, Alberta, Canada: Geo-Slope International Ltd.

Geo-Slope International Ltd. 2007b. SLOPE/W user's guide for slope stability analysis. Calgary, Alberta, Canada: Geo-Slope International Ltd.

Gorum, T., X. Fan, C.J. van Westen, R.Q. Huang, Q. Xu, C. Tang, and G. Wang. 2011. Distribution pattern of earthquake-induced landslides triggered by the 12 May 2008 Wenchuan Earthquake. *Geomorphology* 133: 152–167.

Guo, Z., L. Chen, K. Yin, D.P. Shrestha, and L. Zhang. 2020. Quantitative risk assessment of slow-moving landslides from the viewpoint of decision-making: A case study of the Three Gorges Reservoir in China. *Engineering Geology* 273: Article 105667.

Handwerger, A.L., A.W. Rempel, R.M. Skarbek, J.J. Roering, and G.E. Hilley. 2016. Rate-weakening friction characterizes both slow sliding and catastrophic failure of landslides. *Proceedings of the National Academy of Sciences* 113: 10281–10286.

Handwerger, A.L., J.J. Roering, and D.A. Schmidt. 2013. Controls on the seasonal deformation of slow-moving landslides. *Earth and Planetary Science Letters* 377–378: 239–247.

Horton, A.J., T.C. Hales, C. Ouyang, and X. Fan. 2019. Identifying post-earthquake debris flow hazard using Massflow. *Engineering Geology* 258: Article 105134.

Huang, R., and X. Fan. 2013. The landslide story. *Nature Geoscience* 6: 325–326.

Hungr, O., S. Leroueil, and L. Picarelli. 2014. The Varnes classification of landslide types, an update. *Landslides* 11(2): 167–194.

Huo, J., and Y. Hu. 1992. Study on attention laws of ground motion parameters. *Earthquake Engineering and Engineering Vibration* 12: 1–11.

Jibson, R.W. 2011. Methods for assessing the stability of slopes during earthquakes – A retrospective. *Engineering Geology* 122(1–2): 43–50.

Keefer, D.K. 1984. Landslides caused by earthquakes. *Geological Society of America Bulletin* 95: 406–421.

Korup, O., J.J. Clague, R.L. Hermanns, K. Hewitt, A.L. Strom, and J.T. Weidinger. 2007. Giant landslides, topography, and erosion. *Earth and Planetary Science Letters* 261: 578–589.

Lewkowicz, A.G., and R.G. Way. 2019. Extremes of summer climate trigger thousands of thermokarst landslides in a high arctic environment. *Nature Communications* 10: Article 1329.

Liu, M., N. Chen, and C. Zhao. 2018. Influence of fault structure on debris flow in Qiaojia and Menggu section of the Jinsha River. *Journal of Natural Disasters* 27: 136–143 (in Chinese).

Luo, Y., J.-M. Zhang, Z. Zhou, Z.-J. Shen, L. Chong, and C. Victor. 2021. Investigation and prediction of water infiltration process in cracked soils based on a full-scale model test. *Geoderma* 400: Article 115111.

Malamud, B.D., D.L. Turcotte, F. Guzzetti, and P. Reichenbach. 2004. Landslide inventories and their statistical properties. *Earth Surface Processes and Landforms* 29: 687–711.

Mishra, S.K., and V.P. Singh. 2003. *Soil conservation service curve number (SCS-CN) methodology*. Berlin: Springer.

Ni, H., and Z. Song. 2019. Response of debris flow occurrence to daily rainfall pattern and critical rainfall condition in the Anning River-Zemu River Fault Zone, SW China. *Bulletin of Engineering Geology and the Environment* 79: 1735–1747.

Ouimet, W.B., K.X. Whipple, L.H. Royden, Z. Sun, and Z. Chen. 2007. The influence of large landslides on river incision in a transient landscape: Eastern margin of the Tibetan Plateau (Sichuan, China). *Geological Society of America Bulletin* 119: 1462–1476.

Parker, R.N., A.L. Densmore, N.J. Rosser, M. de Michele, Y. Li, R. Huang, S. Whadcoat, and D.N. Petley. 2011. Mass wasting triggered by the 2008 Wenchuan Earthquake is greater than orogenic growth. *Nature Geoscience* 4: 449–452.

Pascal, L., L.H. Alexander, and B. Grégory. 2020. Life and death of slow-moving landslides. *Nature Reviews Earth & Environment* 1: 404–409.

Podolskiy, E.A., G. Chambon, M. Naaim, and J. Gaume. 2015. Evaluating snow weak-layer failure parameters through inverse finite element modelling of shaking-platform experiments. *Natural Hazards and Earth System Sciences* 15(1): 119–134.

Ram, A.R., M.S. Brook, and S.J. Cronin. 2019. Engineering geomorphological investigation of the Kasavu landslide, Viti Levu, Fiji. *Landslides* 16: 1341–1351.

Reid, M.E., D.L. Brien, R.G. Lahusen, J.J. Roering, and S.D. Ellen. 2003. Debris-flow initiation from large, slow-moving landslides. In *Debris-flow hazards mitigation: Mechanics prediction and assessment*, ed. D. Rickenmann, and C.-L. Chen, 435–445. Rotterdam: Millpress.

Richards, L.A. 1931. Capillary conduction of liquids through porous mediums. *Physics* 1(5): 318–333.

Rivière, J., P. Shokouhi, R.A. Guyer, and P.A. Johnson. 2015. A set of measures for the systematic classification of the nonlinear elastic behavior of disparate rocks. *Journal of Geophysical Research: Solid Earth* 120: 1587–1604.

Samodra, G., D.S. Hadmoko, G.N. Wicaksono, I.P. Adi, M. Yudinugroho, S.B. Wibowo, H. Suryatmojo, and T.H. Purwanto et al. 2018. The March 25 and 29, 2016 landslide-induced debris flow at Clapar, Banjarnegara, Central Java. *Landslides* 15: 1–9.

Scheingross, J.S., B.M. Minchew, B.H. Mackey, M. Simons, and M.P. Lamb. 2013. Fault-zone controls on the spatial distribution of

slow-moving landslides. *Geological Society of America Bulletin* 125: 473–489.

Schoeller, H. 1977. Geochemistry of groundwater. In *Groundwater studies – An International guide for research and practice*, ed. R.H. Brown, A.A. Konoplyantsev, J. Ineson, and V.S. Kovalevsky, 1–18. Paris: UNESCO.

Shi, P., T. Ye, Y. Wang, T. Zhou, W. Xu, J. Du, J. Wang, and N. Li et al. 2020. Disaster risk science: A geographical perspective and a research framework. *International Journal of Disaster Risk science* 11(4): 426–440.

Shoaei, G., and R.C. Sidle. 2009. Variation in soil characteristics and hydrologic properties associated with historic land use near a recent landslide, Nagano Prefecture, Japan. *Geoderma* 153: 37–51.

Sichuan Huadi Construction Engineering Co. Ltd. 2016. Emergency investigation report of debris flows in the Lengzi Gully (in Chinese).

Strom, A.L., and O. Korup. 2006. Extremely large rockslides and rock avalanches in the Tien Shan Mountains, Kyrgyzstan. *Landslides* 3: 125–136.

Tang, C., T.W.J. van Asch, M. Chang, G.Q. Chen, and X.H. Zhao. 2012. Catastrophic debris flows on 13 August 2010 in the Qingping area, southwestern China: The combined effects of a strong earthquake and subsequent rainstorms. *Geomorphology* 139: 559–576.

Tanyas, H., C.J. van Westen, K.E. Allstadt, M. Anna Nowicki Jessee, T. Görüm, R.W. Jibson, J.W. Godt, and H.P. Sato et al. 2017. Presentation and analysis of a worldwide database of earthquake-induced landslide inventories. *Journal of Geophysical Research: Earth Surface* 122: 1991–2015.

Tian, S., N. Chen, H. Wu, C. Yang, Z. Zhong, and M. Rahman. 2020. New insights into the occurrence of the Baige landslide along the Jinsha River in Tibet. *Landslides* 17: 1207–1216.

Tian, C.-S., Y.-P. Fang, L.E. Yang, and C.-J. Zhang. 2019. Spatial-temporal analysis of community resilience to multi-hazards in the Anning River basin, Southwest China. *International Journal of Disaster Risk Reduction* 39: Article 101144.

Tian, Y., L.A. Owen, C. Xu, S. Ma, K. Li, X. Xu, P.M. Figueiredo, and W. Kang et al. 2020. Landslide development within 3 years after the 2015 Mw 7.8 Gorkha earthquake. *Nepal. Landslides* 17: 1251–1267.

Tibet Autonomous Region Geology and Minerals Bureau. 1988. Geological survey report of the People's Republic of China. Lhasa: Tibet Autonomous Region Geology and Minerals Bureau (in Chinese).

Wang, C.Y., L.H. Cheng, C.V. Chin, and S.B. Yu. 2001. Coseismic hydrologic response of an alluvial fan to the 1999 Chi-Chi Earthquake. *Taiwan. Geology* 29(9): Article 831.

Wang, J., J.D. Howarth, E.L. Mcclymont, A.L. Densmore, and R.G. Hilton. 2020. Long-term patterns of hillslope erosion by earthquake-induced landslides shape mountain landscapes. *Science Advances* 6: Article eaaz6446.

Wang, G., Y. Jiang, C. Chang, I. Doi, and T. Kamai. 2019. Volcaniclastic debris avalanche on Motomachi area of Izu-Oshima, Japan, triggered by severe storm: Phenomenon and mechanisms. *Engineering Geology* 251: 24–36.

Wei, Z.-L., Q. Lü, H.-Y. Sun, and Y.-Q. Shang. 2019. Estimating the rainfall threshold of a deep-seated landslide by integrating models for predicting the groundwater level and stability analysis of the slope. *Engineering Geology* 253: 14–26.

Weight, W.D., and J.L. Sonderegger. 2001. *Manual of applied field hydrogeology*. New York: McGraw-Hill.

Wu, L.Z., Y. Zhou, P. Sun, J.S. Shi, G.G. Liu, and L.Y. Bai. 2017. Laboratory characterization of rainfall-induced loess slope failure. *CATENA* 150: 1–8.

Xu, Z., and W. Liu. 2011. Some problems in the study of the genesis of Xigeda Formation. *Earth Science Frontiers* 18: 256–270 (in Chinese).

Xu, Q., W. Li, X. Li, X. Xiao, X. Fan, and X. Pei. 2017. The Xinmocun landslide on June 24, 2017 in Maoxian, Sichuan: Characteristics and failure mechanism. *Chinese Journal of Rock Mechanics and Engineering* 36: 2612–2628 (in Chinese).

Xu, Q., H.X. Liu, J.X. Ran, W.H. Li, and X. Sun. 2016. Field monitoring of groundwater responses to heavy rainfalls and the early warning of the Kualiangzi landslide in Sichuan Basin, southwestern China. *Landslides* 13(6): 1–16.

Yang, R., H.A. Suhail, L. Gourbet, S.D. Willett, M.G. Fellin, X. Lin, J. Gong, and X. Wei et al. 2020. Early Pleistocene drainage pattern changes in eastern Tibet: Constraints from provenance analysis, thermochronometry, and numerical modeling. *Earth and Planetary Science Letters* 531: Article 115955.

Yang, Z., X. Zhao, M. Chen, J. Zhang, Y. Yang, W. Chen, X. Bai, M. Wang, and Q. Wu. 2023. Characteristics, dynamic analyses and hazard assessment of debris flows in Niumiangou Valley of Wenchuan County. *Applied Sciences* 13: Article 1161.

Zhang, Y., Y. Cheng, Y. Yin, H. Lan, J. Wang, and X. Fu. 2014. High-position debris flow: A long-term active geohazard after the Wenchuan Earthquake. *Engineering Geology* 180: 45–54.

Zhang, S., R. Li, F. Wang, and A. Iio. 2019. Characteristics of landslides triggered by the 2018 Hokkaido Eastern Iburi earthquake, northern Japan. *Landslides* 16: 1691–1708.

Zhou, D. 2019. *Applicability analysis of attenuation relation of ground motion in western of China. Master's thesis*. Beijing: China Earthquake Administration.

Zienkiewicz, O.C., and K.G. Stagg. 1969. *Rock mechanics in engineering practice: Influence of interstitial water on the behaviour of rock masses*. London: Wiley.